Microelectronics Journal 148 (2024) 106191

Contents lists available at ScienceDirect

Microelectronics Journal

journal homepage: www.elsevier.com/locate/mejo

Suppressed current collapse and improved threshold voltage stability of AlGaN/GaN HEMT via O_2 plasma treatment

Yitai Zhu [a], Yu Zhang [a,b,c], Haolan Qu [a,b,c], Han Gao [a], Haitao Du [a], Haowen Guo [a], Xinbo Zou [a,*]

[a] School of Information Science and Technology (SIST), ShanghaiTech University, Shanghai, China
[b] School of Microelectronics, University of Chinese Academy of Sciences, Beijing, China
[c] Shanghai Institute of Microsystem and Information Technology, Shanghai, China

ARTICLE INFO

Keywords:
AlGaN/GaN HEMT
O_2 plasma treatment
Current collapse
Threshold voltage shift
Dynamic characteristic

ABSTRACT

A comprehensive study about the effects of O_2 plasma treatment on the dynamic performance of AlGaN/GaN high electron mobility transistors (HEMTs) is presented. The drain current transient spectroscopy indicated a much decelerated and mitigated current degradation process for the HEMT with O_2 plasma treatment. Upon negative gate bias stressing, current collapse of 10.7 % and minor threshold voltage shift of 0.16 V were achieved by O_2 plasma treatment. In addition, current collapse ratio of the HEMTs as a function of stress/recovery time showed that the HEMT with O_2 plasma treatment had a superior performance in various on-off conditions. Particularly in high-frequency switching events, current collapse ratio was reduced from about 50 % to 0.2 %. At last, the quality of AlGaN/metal interface with O_2 plasma treatment is demonstrated by capacitance-frequency measurements, with the interface trap density D_{it} is estimated to be 1.39×10^{12} cm^{-2} eV^{-1}. These results indicate that GaN HEMT with O_2 plasma treatment is a promising technology in power switching applications.

1. Introduction

Among gallium nitride (GaN) devices, high electron mobility transistors (HEMTs) are promising candidates for next-generation high-frequency and high-power applications due to their exceptional material properties, including wide bandgap, high saturation electron mobility, high critical breakdown electric field, and ability to operate at high temperatures [1,2]. However, the undesirable properties of the devices in power conversion like current collapse and threshold voltage shift limit the application of HEMT [3–6]. Numerous studies have established that the primary cause of the undesirable properties is associated with the defects and surface traps arising from the device fabrication process [7,8]. To mitigate this problem, various plasma treatments had been applied to improve surface quality of HEMTs, such as CF_4 plasma treatment [9–11], N_2O plasma treatment [12–14], O_2 plasma treatment [15–26], and so on.

Among these options, O_2 plasma treatment is widely utilized due to its cost-effectiveness and easy implementation. Recently studies have demonstrated the virtue of O_2 plasma treatment in enhancing the performance of GaN-based devices. For instance, Liu et al. fabricated quasi-vertical GaN SBD on a sapphire substrate based on O_2 plasma treatment [20], improving the breakdown voltage from 80 V to 180 V and achieving a four-orders reduction of reverse leakage current. Walid Amir et al. used O_2 plasma treatment before gate metal deposition to enhance the RF performance of AlGaN/GaN HEMT [25]. The device with O_2 plasma treatment had an enhancement in P_{out_max} from 1.25 W/mm to 2.4 W/mm. Wang et al. fabricated AlGaN/GaN MIS-HEMTs using O_2 plasma treated Al_2O_3 as gate dielectric and reported improvement in dynamic R_{on} [26].

Despite that the DC and preliminary dynamic performances of GaN HEMTs with O_2 plasma treatment have been studied, detailed dynamic characteristics resulting from O_2 plasma treatment, including threshold voltage shift and time-resolved drain current degeneration have not been thoroughly investigated. Moreover, the relationship between dynamic performance in different on-off conditions and the trap capture/emission behavior still remain unclear.

In this work, an explicit study on dynamic performances of GaN HEMT with O_2 plasma treatment is presented. Firstly, time-resolved drain current (I_d) was investigated by drain current transient (DCT) spectroscopy. Subsequently, the current collapse and threshold voltage instabilities of devices upon various gate biases were demonstrated. In addition, the collapse ratio of current was extracted as a function of stress time and recovery time to correlate the trap behavior with various operating conditions. Finally, capacitance-frequency (C-f)

* Corresponding author.
E-mail address: zouxb@shanghaitech.edu.cn (X. Zou).

https://doi.org/10.1016/j.mejo.2024.106191
Received 18 January 2024; Received in revised form 25 March 2024; Accepted 2 April 2024
Available online 9 April 2024
1879-2391/

measurements were used to characterize the interface states between AlGaN and metal, demonstrating a lower interfacial trap density (D_{it}) compared to other surface treatment processes. The results show that O_2 plasma treatment is a promising technology in enabling high dynamic performance of GaN HEMT for power switching applications.

2. Device fabrication

Fig. 1 (a) showed the schematic cross section of the GaN HEMT structure employed in this study. The GaN HEMT was grown on a 6-inch Si (111) substrate by metal-organic chemical vapor deposition (MOCVD). The epitaxial layer stack comprised a 3 μm-thick buffer layer, a 200 nm undoped GaN channel layer, a 1 nm AlN spacer layer, a 25 nm undoped $Al_{0.25}Ga_{0.75}N$ layer, and a 3 nm GaN cap layer. As shown in Fig. 1 (b), device fabrication process commenced with mesa isolation achieved through Cl-based plasma etching. Ohmic contacts were formed by sequential deposition of 20/50/150/80 nm Ti/Al/Ni/Au layers, followed by annealing at 850 °C in N_2 for 40 s. Subsequently, three cycles of O_2 plasma treatment were performed. Etch cycle consisted of a 1-min O_2 plasma treatment with a low RF power of 100W, followed by a 2-min immersion in dilute HCl. The treatment process is to remove imperfect surface layer, as well as eliminate donor-level nitrogen vacancies and leakage paths [27]. Finally, 20/200 nm Ni/Au gate metal was deposited. The gate length (L_g), gate-source distance (L_{gs}), gate-drain distance (L_{gd}), and gate width (W_g), of the devices were 1/2/2/20 μm, respectively. The conventional HEMT underwent the same fabrication process, except for the O_2 plasma treatment serving as a basis for comparison.

3. Result and discussion

3.1. Static DC characteristics

Fig. 2(a) illustrated the transfer characteristics of AlGaN/GaN HEMTs with and without O_2 plasma treatment at room temperature. The threshold voltages (V_{th}) of HEMTs were extracted to be −2.78 V (without treatment) and −3.2 V (with treatment) at V_{ds} = 3 V, defined at I_d of 1 mA/mm from the transfer curves. The HEMT with treatment exhibited a four orders lower leakage current compared with the HEMTs without treatment, which clearly demonstrates the effectiveness of O_2 treatment in suppressing off-state leakage currents. Moreover, the subthreshold slop (SS) of the device was improved from 142 mV/dec to 70 mV/dec due to the reduction of leakage currents. Fig. 2(b) showed output characteristics of both HEMTs. The device with treatment exhibited a higher saturation current density of 446 mA/mm and a smaller R_{ON} value of 5.16 Ω mm extracted at (V_{gs} -V_{th}) = 3.2 V. In contrast, the saturation current density and R_{ON} of the device without treatment were extracted to be 375 mA/mm and 5.37 Ω mm, respectively. The differences in DC characteristics were due to the reduction of electrons captured by surface trap upon surface treatment, leading to a slight increase of channel carrier density.

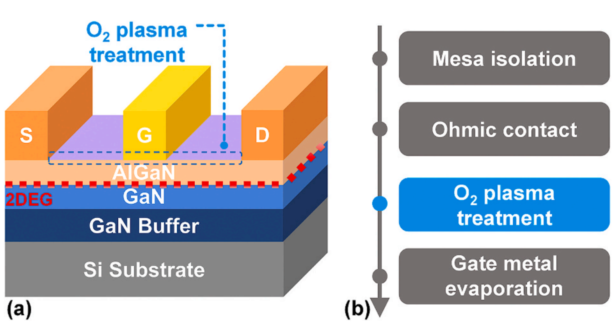

Fig. 1. (a) Schematic structures and (b) fabrication scheme of the AlGaN/GaN HEMT with O_2 plasma treatment.

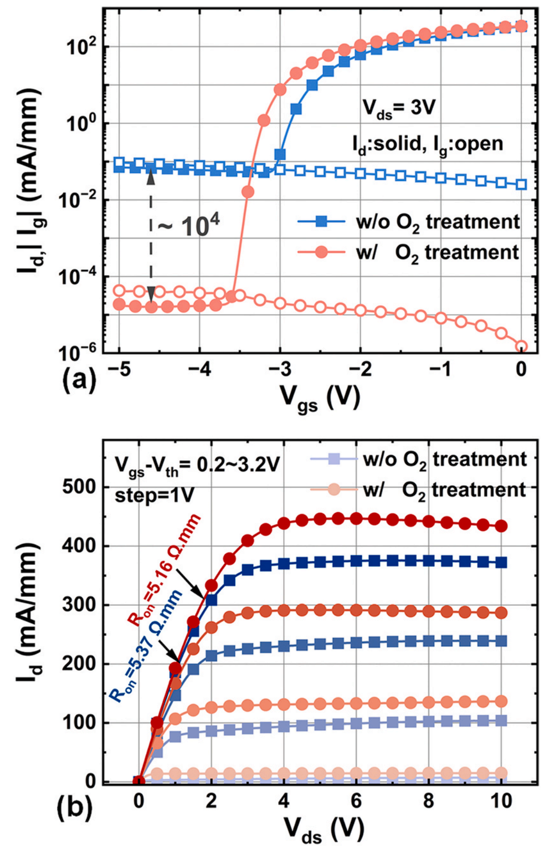

Fig. 2. (a) Log-scale transfer characteristics at V_{ds} = 3 V and Log-scale gate leakage current at V_{ds} = 3 V. (b) Output characteristics at V_{gs}-V_{th} from 0.2 V to 3.2 V of AlGaN/GaN HEMT without O_2 treatment (blue line) and with O_2 treatment (red line).

3.2. Dynamic performance

Fig. 3 showed the drain current transients (DCT) spectroscopy with a negative gate stressing voltage ($V_{gs,stress}$) of −3 V for a stressing time of 1s. The $V_{gs,stress}$ was defined as the gate bias voltage minus the threshold voltage (V_{th}). In this stressing condition, the gate-induced trapping (mainly caused by the surface traps) will be the dominating factor of the current degradation. The normalized I_d is presented, which was defined as the ($I_{d,dynamic}$/$I_{d,static}$), where $I_{d,static}$ was measured in the non-stressed fresh state [(V_{gs},V_{ds}) = (−0.5 V, 1 V)]. As shown in Fig. 3, the normalized I_d of the HEMT without treatment rapidly degraded within 10 μs

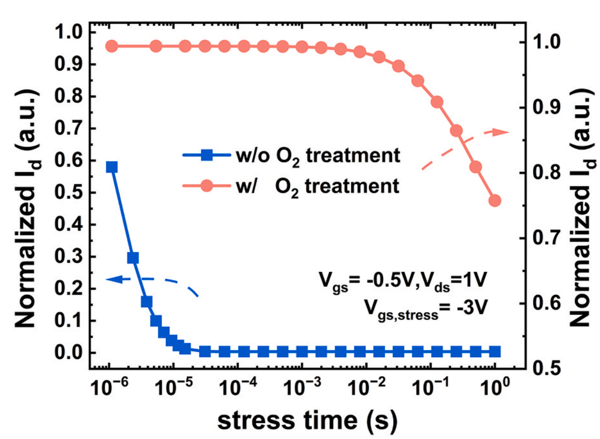

Fig. 3. Drain current transients within 1s stressing process for gate stressing voltage = −3 V. The drain current was measured at V_{gs} = −0.5 V and V_{ds} = 1 V.

and the degradation ratio close to 100 %. In contrast, the HEMT with treatment, exhibited little change in drain current within 10 μs and followed with a gradual decrease after 1 ms. After the device was exposed to $V_{gs,stress} = -3$ V for 1 s, a normalized I_d of 0.75 can be obtained. When the device was exposed to the negative gate stressing voltage, the electrons injected from gate will be captured in the trap states, compensating the donor atoms and depleting the channel between the gate and the drain, leading to the decrease of I_d. A faster degradation rate in HEMT without treatment can be observed compared with the HEMT with treatment.

The DCT signal was fitted as a function represented by a sum of exponential decays to investigate the trapping time constants (τ) of the two HEMTs. The fitting function can be expressed as [28,29]:

$$I_{fitted} = \sum_{i=1}^{n} A_i \, exp\left(\frac{-t}{\tau_i}\right) + I_{final}$$

where τ_i is the typical time constant, and A_i is the amplitude of each exponential decay function associated to the relative time constant τ_i. The capture time constant (τ_c) of 1.18 μs and 470 ms could be extracted for the untreated and treated HEMT, respectively. The capture time constant of the HEMT with treatment is 5 orders larger than HEMT without treatment. The difference between the capture time constant was due to the suppressed “fast” (shallow) traps of treated HEMT. It is reported that low-quality surface layer could induce “fast traps” and proper surface treatment is demanding for their elimination [30].

Fig. 4 showed pulsed output characteristics of devices with various $V_{gs,stress}$. During stress phase, gate was applied with a negative $V_{gs,stress}$ while source and drain were grounded to common voltage. The pulse period and pulse width were set to 100 μs and 1 μs, respectively. As shown in Fig. 4(a), the saturation drain current decreased when the negative $V_{gs,stress}$ was biased to the HEMT with treatment. When $V_{gs,stress} = -3$ V, a small current collapse of 1.29 % can be observed. Even $V_{gs,stress}$ increased to −7 V, the current collapse remained relatively low at 10.7 %. In contrast, the pulsed transfer characteristic of HEMT without treatment was shown in Fig. 4(b). As $V_{gs,stress} = -3$ V, a current collapse of 67.5 % was extracted. When the negative $V_{gs,stress}$ was strengthened, the severer current collapse occurred, which increased to 77.8 % as the $V_{gs,stress} = -7$ V. Compared to the HEMT with treatment, the HEMT without treatment exhibited relatively higher current collapse in all $V_{gs,stress}$ conditions. The reasons for this phenomenon were due to the HEMT with treatment had a larger capture time constant and it exhibited a slower rate of electron capture by surface traps when subjected to negative gate voltage stress. Conversely, the untreated HEMT, with a shorter time constant, experiences a more rapid capture of electrons, resulting in more serious current collapse and ΔV_{th}.

Fig. 5(a) displayed threshold voltage instability of treated HEMT induced by negative gate voltage stressing condition, with $V_{gs,stress}$ ranging from −3 V to−7 V. When negative $V_{gs,stress}$ was applied, the threshold voltage was shifted positively. A small ΔV_{th} of 0.03 V can be obtained when $V_{gs,stress} = -3$ V. And ΔV_{th} only increased to 0.16 V as $V_{gs,stress}$ enhanced to −7 V. Fig. 5(b) showed threshold voltage instability of untreated HEMT in the same negative gate voltage conditions. In this case, a larger ΔV_{th} of 0.34 V was observed at the $V_{gs,stress}$ = -3 V. When $V_{gs,stress}$ was increased to −7 V, the positive shift in threshold voltage was further aggravated, resulting in a $\Delta V_{th} = 0.58$ V. Fig. 5(c) summarized the ΔV_{th} as a function of the $V_{gs,stress}$, the ΔV_{th} were summarized from Fig. 5(a)–(b). The amplitude of the ΔV_{th} was significantly reduced for the HEMT with treatment in all $V_{gs,stress}$ conditions. Especially when $V_{gs,stress} = -7$ V, the ΔV_{th} was reduced from 0.58 V to 0.16 V, which highlighting the superior threshold voltage stability of HEMT with treatment. The positive shift of threshold voltage was related to the electrons trapping by surface traps. When negative gate stress was applied to the device, the electrons was captured by surface traps state, result in depleting the electron density in the conductive channel and causing a positive shift in the threshold voltage. When an enhanced negative gate stress was applied, a larger ΔV_{th} can be obtained. However, the HEMT with O_2 plasma treatment exhibits improved surface quality, leading to a reduction in the number of electrons captured by the surface state and an improved V_{th} reliability.

Fig. 6 reported the transient of current collapse for both HEMTs during stress and recovery processes. The waveform schematic of transient measurement consisted of stress and recovery processes was shown in Fig. 6 (a). The duration of stress process($t_{s,max}$) ranged from 250 ns to 1 s and after different stress processes followed by a recovery process with a constant duration of 1s. During stress process the devices were biased at the negative gate stressing condition of ($V_{gs,stress}$, $V_{ds,stress}$) =

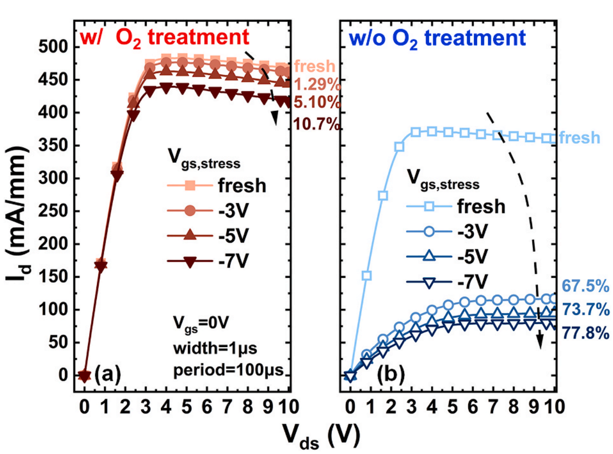

Fig. 4. Pulsed output characteristics of HEMTs (a) with treatment and (b) without treatment at different gate stressing voltage with 1-μs pulse width and 100-μs pulse period. The measurement V_{gs} was 0 V.

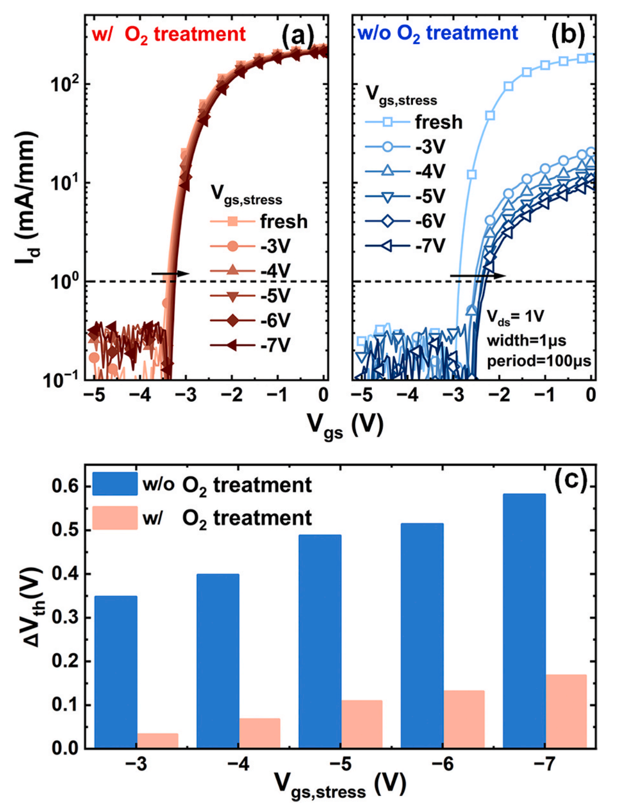

Fig. 5. Pulsed transfer characteristics of HEMTs (a) with treatment and (b) without treatment at different gate stressing voltage. (c) Dependence of the threshold voltage shift (ΔV_{th}) versus negative gate voltage ($V_{gs,stress}$).

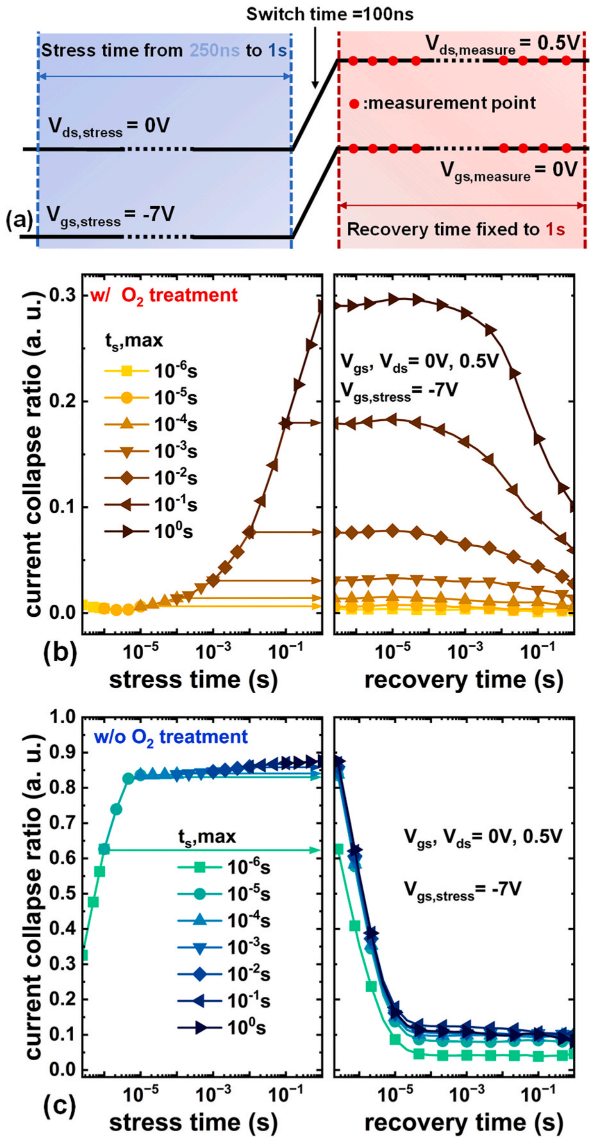

Fig. 6. (a) Waveform schematic of current collapse transient measurement. Current collapse transients of HEMT (b) with (c) without treatment, recovery time was fixed at 1s while maximum stress times $t_{s,max}$ changed from 250ns to 1s, ($V_{gs,stress}$, $V_{ds,stress}$) = (−7 V, 0 V), ($V_{gs,measure}$, $V_{ds,measure}$) = (0 V, 0.5 V).

(−7 V, 0 V), the bias voltage was remained constant and no measurement was performed. In the recovery process the bias voltage was switched to measuring voltage ($V_{gs,measure}$, $V_{ds,measure}$) = (0 V, 0.5 V). Setting gate to zero bias and applying a small drain voltage ensured that the device was in a recovery process while the measurement was carried out. In addition, the small drain voltage could avoid the hot electron effect and ensure the full recovery of the current. Since the fast switch, the current at the first measurement point basically did not recover during this time. C.C ratio transient in stress process was extracted by varying $t_{s,max}$ from 250 ns to 1 s. Fig. 6(b)-(c) illustrated the current collapse transient for both HEMTs. For the HEMT with treatment the capture and emission processes of the trap continued within a measurement window of 1 s. When $t_{s,max} < 1$ ms, a micro current collapse ratio about 3 % was observed. Even at $t_{s,max} = 1$ s, the maximum current collapse ratio was only 28 %. In contrast, for the HEMT without treatment the capture and emission processes of the trap quickly reached saturation within 10 μs. When the $t_{s,max} = 1$ μs, the current collapse ratio was 80 %, and gradually rising to 90 % at $t_{s,max}$ = 1 s. In recovery process, the HEMT with treatment showed a slower change rate compared with the HEMT without treatment. The emission time constants of 175 ms and 3.94 μs could be extracted for HEMT with treatment and without treatment, respectively. The results indicated the differences in time constants between treated/untreated HEMTs, with treated HEMT showing a better stability. To further investigate the device degradation with practical operating conditions, the contour plots of current collapse was plotted.

Fig. 7 presented the current collapse ratio (C.C ratio) as function of stress time (t_{off}) and recovery time (t_{on}). Iso-frequency and iso-duty-cycle line were marked to evaluate the dynamic behavior of the GaN HEMT with different on-off conditions. As shown in Fig. 7(a), the contour plot of current collapse for HEMT with treatment could be divided into three regions:

Region I: $t_{off} < 1$ ms. The peak value of current collapse ratio in this region is below 3 %. Current collapse effect is negligible due to the small stress time t_{off} which is much shorter than trap time constant (420 ms), resulting in few electrons captured by surface trap state.

Region II: $t_{on} < 1$ ms, $t_{off} > 1$ ms. As the stress time increases from 1 ms to 1 s, current collapse ratio deteriorated from 3 % to 29.3 %. The current collapse can be attributed to the trap capture process. Moreover, when $t_{off} < 1$ ms, almost no electrons were released, so the extending of t_{on} has little or no significant improvement on current collapse.

Region III: $t_{on} > 1$ ms, $t_{off} > 1$ ms. Compared to region II, the recovery rate of current collapse accelerated in this region. When t_{off} = 1s with t_{on} was verified from 1 ms to 1 s, current collapse ratio recovered from 29.7 % to 10 %. When the t_{on} increased, the release of electrons becomes more complete, resulting in current recovery.

As shown in Fig. 7(b), the contour plot of current collapse for HEMT without treatment also divided into three regions. Owing to the smaller time constant, capture and emission processes of traps were completed in a shorter time, with the boundary time of 10 μs. In region I, current

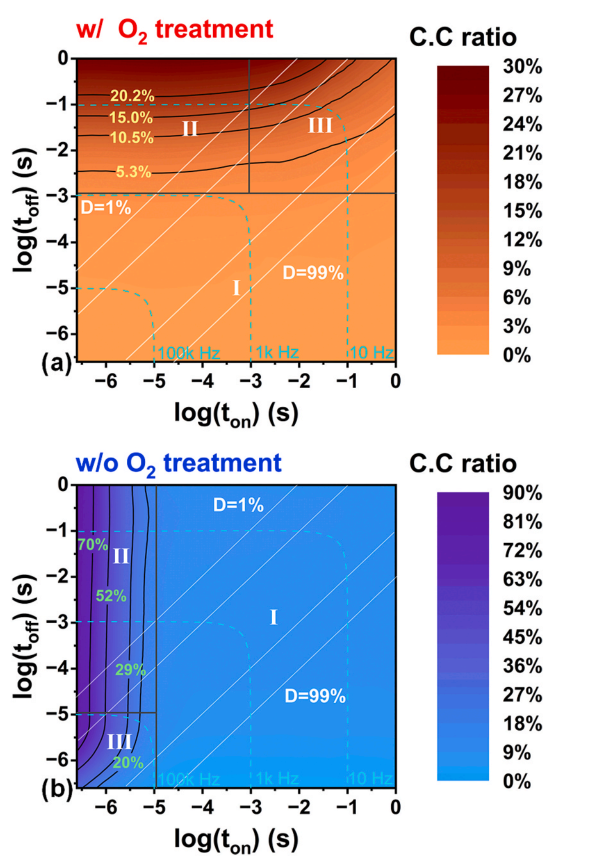

Fig. 7. Contour plot showing the dependency of the current collapse ratio on t_{on} and t_{off}, together with the iso-frequency and iso-duty-cycle line.

collapse was relatively small, generally below 10 %, since the small time constant. In region II and III, a more severe current collapse could be observed with an increase of t_{off} before t_{off} = 10 μs. The peak current collapse ratio reached 86.5 % when t_{off} = 1 μs and t_{on} = 250 ns. In summary, with different duty cycle and frequency combinations, particularly at higher frequencies (>100 kHz) and lower duty cycle (<50 %), current collapse ratio was reduced from about 50 % to 0.2 % by the O_2 plasma treatment, due to the better surface quality. Consequently, the HEMT with treatment had an improved behavior across a wide range of operating conditions.

As shown in Fig. 8, the trap density D_{it} was extracted by the capacitance-frequency (C-f) method for the SBD which had the same fabrication process. The capacitance decreases from 70 pF to 0.3 pF as the frequency increases from 1 kHz to 5 MHz. The reduction in capacitance is related to the capture and emission processes of electrons in the traps. The total capacitance at high frequencies (C_{HF}) only included the depletion capacitance (C_D), which could be described as $C = C_D$. At low frequencies, more surface traps responded to the signal and contributed to capacitance. The total capacitance at low frequency (C_{LF}) was the sum of the depletion capacitance (C_D) and the interface capacitance (C_{it}), which can be described as $C = C_D + C_{it}$. And the surface trap density (D_{it}) can be extracted by $D_{it} = C_{it}/(q^2A) = (C_{LF}\text{-}C_{HF})/(q^2A)$ [28], where A is the junction area, C_{LF} and C_{HF} are the capacitances at low and high frequencies, respectively. The D_{it} for the HEMT with treatment was estimated to be 1.39×10^{12} cm^{-2} eV^{-1}. Table 1 presents a comparison of D_{it} between this work and other devices subject to different treatment processes. Devices with other plasma treatment processes, such as N_2O plasma treatment [12] and O_2 plasma treatment [24] exhibited the D_{it} of 4.78×10^{12} cm^{-2} eV^{-1} and 2.9×10^{12} cm^{-2} eV^{-1}, respectively. A device with 1-min piranha cleaning showed a D_{it} of 1.51×10^{12} cm^{-2} eV^{-1} [29]. In this study, a D_{it} of 1.39×10^{12} cm^{-2} eV^{-1} was achieved with O_2 plasma treatment. These results indicated that the HEMT with treatment in this work exhibits a good surface quality for reliable power switching applications.

4. Conclusion

DC and dynamic performances of the GaN HEMTs with/without O_2 plasma treatment were thoroughly investigated and compared. The off-state leakage current exhibited a significant reduction of approximately four orders of magnitude, while the saturation current density increased by 24 % after the O_2 plasma treatment. In terms of dynamic characteristics, after O_2 plasma treatment the current collapse ratio reduced from 77.8 % to 10.7 % and positive threshold voltage shift improved from 0.58 V to 0.16 V when a negative stressing voltage of −7 V was applied to gate. These improvements could be attributed to the improvement of surface quality and reduction of surface trap density achieved through the O_2 plasma treatment. Additionally, the transient behavior of the current collapse was extracted as a function of stress time and recovery time to accurately reproduce the capture/emission behavior with various operating conditions. Within the measurement range, the HEMT with O_2 plasma treatment demonstrated a smaller current degeneration, especially in the high-frequency conditions reaching an optimized current collapse ratio of 0.2 %. Finally, the D_{it} for SBD with O_2 plasma treatment was determined to be 1.39×10^{12} cm^{-2} eV^{-1}. These results proved the potential of GaN HEMTs with O_2 plasma treatment as a promising technology for high-power switching applications.

Declaration of competing interest

The authors declare that they have no known competing financial interests or personal relationships that could have appeared to influence the work reported in this paper.

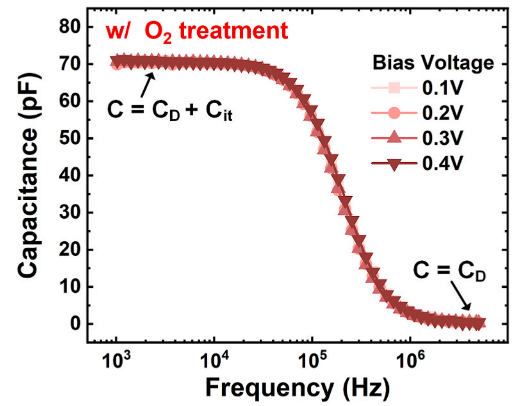

Fig. 8. Capacitance-frequency curves measured at various forward voltages for GaN/AlGaN SBD with O_2 treatment.

Table 1
D_{it} values measured for different surface treatment processes on devices.

Ref	Treatment	Method	D_{it}($cm^{-2}eV^{-1}$)
This work	O_2 plasma	HI-LO	1.39×10^{12}
[12]	N_2O Plasma	Freq. dep. CV	4.78×10^{12}
[24]	O_2 plasma	Freq. dep. CV	$2.9 \times 10^{12*}$
[31]	Piranha cleaning	Conductance	1.51×10^{12}

*Estimated value.

Data availability

Data will be made available on request.

Acknowledgment

This work was supported in part by ShanghaiTech University Startup Fund under Grant 2017F0203-000-14, in part by the National Natural Science Foundation of China under Grant 52131303.

The authors would like to thank ShanghaiTech Quantum Device Laboratory (SQDL).

References

[1] M. Meneghini, C. De Santi, I. Abid, M. Buffolo, M. Cioni, R.A. Khadar, L. Nela, N. Zagni, A. Chini, F. Medjdoub, G. Meneghesso, G. Verzellesi, E. Zanoni, E. Matioli, GaN-based power devices: physics, reliability, and perspectives, J. Appl. Phys. 130 (2021) 181101, https://doi.org/10.1063/5.0061354.

[2] N. Keshmiri, D. Wang, B. Agrawal, R. Hou, A. Emadi, Current status and future trends of GaN HEMTs in electrified transportation, IEEE Access 8 (2020) 70553–70571, https://doi.org/10.1109/ACCESS.2020.2986972.

[3] Y. Zhang, Y. Gu, J. Chen, Y. Zhu, B. Chen, H. Jiang, K.M. Lau, X. Zou, Small V_{th} shift and low dynamic Ron in GaN MOSHEMT with ZrO_2 gate dielectric, IEEE Trans. Electron. Dev. 70 (2023) 5590–5595, https://doi.org/10.1109/TED.2023.3313999.

[4] E. Acurio, F. Crupi, P. Magnone, L. Trojman, G. Meneghesso, F. Iucolano, On recoverable behavior of PBTI in AlGaN/GaN MOS-HEMT, Solid State Electron. 132 (2017) 49–56, https://doi.org/10.1016/j.sse.2017.03.007.

[5] B. Li, Q. Jiang, S. Liu, C. Liu, K.J. Chen, Degradation of transient OFF-state leakage current in AlGaN/GaN HEMTs induced by ON-state gate overdrive, Phys. Status Solidi C 11 (2014) 928–931, https://doi.org/10.1002/pssc.201300445.

[6] Y. Gu, W. Huang, Y. Zhang, J. Sui, Y. Wang, H. Guo, J. Zhou, B. Chen, X. Zou, Temperature-dependent dynamic performance of p-GaN gate HEMT on Si, IEEE Trans. Electron. Dev. 69 (2022) 3302–3309, https://doi.org/10.1109/TED.2022.3167342.

[7] R.J. Shul, L. Zhang, A.G. Baca, C.G. Willison, J. Han, S.J. Pearton, K.P. Lee, F. Ren, Inductively coupled high-density plasma-induced etch damage of GaN MESFETs, Solid State Electron. 45 (2001) 13–17, https://doi.org/10.1016/S0038-1101(00)00164-7.

[8] L. He, L. Li, F. Yang, Y. Zheng, J. Zhang, T. Que, Z. Liu, J. Zhang, Q. Wu, Y. Liu, Correlating device behaviors with semiconductor lattice damage at MOS interface by comparing plasma-etching and regrown recessed-gate Al_2O_3/GaN MOS-FETs, Appl. Surf. Sci. 546 (2021) 148710, https://doi.org/10.1016/j.apsusc.2020.148710.

[9] W. Jin Ha, S. Chhajed, S. Jae Oh, S. Hwang, J. Kyu Kim, J.-H. Lee, K.-S. Kim, Analysis of the reverse leakage current in AlGaN/GaN Schottky barrier diodes treated with fluorine plasma, Appl. Phys. Lett. 100 (2012) 132104, https://doi.org/10.1063/1.3697684.
[10] N.-H. Lee, M. Lee, W. Choi, D. Kim, N. Jeon, S. Choi, K.-S. Seo, Effects of various surface treatments on gate leakage, subthreshold slope, and current collapse in AlGaN/GaN high-electron-mobility transistors, Jpn. J. Appl. Phys. 53 (2014) 04EF10, https://doi.org/10.7567/JJAP.53.04EF10.
[11] R. Chu, L. Shen, N. Fichtenbaum, D. Brown, S. Keller, U.K. Mishra, Plasma treatment for leakage reduction in AlGaN/GaN and GaN Schottky contacts, IEEE Electron. Device Lett. 29 (2008) 297–299, https://doi.org/10.1109/LED.2008.917814.
[12] J. Chen, J. Qin, W. Xiao, H. Wang, Effective suppression of current collapse in AlGaN/GaN HEMT with N_2O plasma treatment followed by high temperature annealing in N_2 ambience, IEEE J. Electron Devices Soc. 10 (2022) 356–360, https://doi.org/10.1109/JEDS.2022.3169811.
[13] Y. He, Q. He, M. Mi, M. Zhang, C. Wang, L. Yang, X. Ma, Y. Hao, High breakdown electric field MIS-free fully recessed-gate normally off AlGaN/GaN HEMT with N_2O plasma treatment, IEEE J. Emerg. Sel. Top. Power Electron. 9 (2021) 2163–2170, https://doi.org/10.1109/JESTPE.2019.2940594.
[14] M.-H. Mi, X.-H. Ma, L. Yang, Y. Lu, B. Hou, M. Zhang, H.-S. Zhang, S. Wu, Y. Hao, Record combination f max · V br of 25 THz·V in AlGaN/GaN HEMT with plasma treatment, AIP Adv. 9 (2019) 045212, https://doi.org/10.1063/1.5090528.
[15] X. Lu, H. Jiang, C. Liu, X. Zou, K.M. Lau, Off-state leakage current reduction in AlGaN/GaN high electron mobility transistors by combining surface treatment and post-gate annealing, Semicond. Sci. Technol. 31 (2016) 055019, https://doi.org/10.1088/0268-1242/31/5/055019.
[16] J.A. Bardwell, S. Haffouz, W.R. McKinnon, C. Storey, H. Tang, G.I. Sproule, D. Roth, R. Wang, The effect of surface cleaning on current collapse in AlGaN / GaN HEMTs, Electrochem. Solid State Lett. 10 (2006) H46, https://doi.org/10.1149/1.2402479.
[17] A. Calzolaro, N. Szabó, A. Großer, J. Gärtner, T. Mikolajick, A. Wachowiak, Surface preconditioning and postmetallization anneal improving interface properties and V_{th} stability under positive gate bias stress in AlGaN/GaN MIS-HEMTs, Phys. Status Solidi A 218 (2021) 2000585, https://doi.org/10.1002/pssa.202000585.
[18] D.S. Lee, J.W. Chung, H. Wang, X. Gao, S. Guo, P. Fay, T. Palacios, 245-GHz InAlN/GaN HEMTs with oxygen plasma treatment, IEEE Electron. Device Lett. 32 (2011) 755–757, https://doi.org/10.1109/LED.2011.2132751.
[19] J.T. Asubar, Y. Sakaida, S. Yoshida, Z. Yatabe, H. Tokuda, T. Hashizume, M. Kuzuhara, Impact of oxygen plasma treatment on the dynamic on-resistance of AlGaN/GaN high-electron-mobility transistors, Appl. Phys. Express 8 (2015) 111001, https://doi.org/10.7567/APEX.8.111001.
[20] J. Liu, C. Han, W. Liu, L. Geng, Y. Hao, Leakage reduction of quasi-vertical GaN Schottky barrier diode with post oxygen plasma treatment, IEEE Trans. Electron. Dev. 69 (2022) 6929–6933, https://doi.org/10.1109/TED.2022.3212336.
[21] Z. Zheng, W. Song, L. Zhang, S. Yang, J. Wei, K.J. Chen, High I_{ON} and I_{ON}/I_{OFF} ratio enhancement-mode buried p-channel GaN MOSFETs on p-GaN gate power HEMT platform, IEEE Electron. Device Lett. 41 (2020) 26–29, https://doi.org/10.1109/LED.2019.2954035.
[22] J.W. Chung, J.C. Roberts, E.L. Piner, T. Palacios, Effect of gate leakage in the subthreshold characteristics of AlGaN/GaN HEMTs, IEEE Electron. Device Lett. 29 (2008) 1196–1198, https://doi.org/10.1109/LED.2008.2005257.
[23] B.B. Upadhyay, K. Takhar, J. Jha, S. Ganguly, D. Saha, Surface stoichiometry modification and improved DC/RF characteristics by plasma treated and annealed AlGaN/GaN HEMTs, Solid State Electron. 141 (2018) 1–6, https://doi.org/10.1016/j.sse.2017.11.001.
[24] S. Xu, Y. Zhou, X. Zhang, Q. Li, J. Liu, H. Qie, Q. Wang, X. Zhan, X. Sun, Q. Dai, G. Yan, Q. Sun, H. Yang, Effects of ammonia and oxygen plasma treatment on interface traps in AlGaN/GaN metal–insulator–semiconductor high-electron-mobility transistors, Appl. Phys. Lett. 123 (2023) 203504, https://doi.org/10.1063/5.0172364.
[25] W. Amir, J.-W. Shin, K.-Y. Shin, S. Chakraborty, C.-Y. Cho, J.-M. Kim, S.-T. Lee, T. Hoshi, T. Tsutsumi, H. Sugiyama, H. Matsuzaki, D.-H. Kim, T.-W. Kim, Performance enhancement of AlGaN/GaN HEMT via trap-state improvement using O_2 plasma treatment, IEEE Trans. Electron. Dev. 70 (2023) 2988–2993, https://doi.org/10.1109/TED.2023.3268626.
[26] Q. Wang, M. Pan, P. Zhang, L. Wang, Y. Yang, X. Xie, H. Huang, X. Hu, M. Xu, O_2 plasma alternately treated ALD-Al_2O_3 as gate dielectric for high performance AlGaN/GaN MIS-HEMTs, IEEE Access 12 (2024) 16089–16094, https://doi.org/10.1109/ACCESS.2023.3347810.
[27] Shuxun Lin, Maojun Wang, Bing Xie, C.P. Wen, Min Yu, Jinyan Wang, Yilong Hao, Wengang Wu, Sen Huang, K.J. Chen, Bo Shen, Reduction of current collapse in GaN high-electron mobility transistors using a repeated ozone oxidation and wet surface treatment, IEEE Electron. Device Lett. 36 (2015) 757–759, https://doi.org/10.1109/LED.2015.2445495.
[28] J. Joh, J.A. del Alamo, A current-transient methodology for trap analysis for GaN high electron mobility transistors, IEEE Trans. Electron. Dev. 58 (2011) 132–140, https://doi.org/10.1109/TED.2010.2087339.
[29] D. Bisi, M. Meneghini, C. de Santi, A. Chini, M. Dammann, P. Brückner, M. Mikulla, G. Meneghesso, E. Zanoni, Deep-level characterization in GaN HEMTs-Part I: advantages and limitations of drain current transient measurements, IEEE Trans. Electron. Dev. 60 (2013) 3166–3175, https://doi.org/10.1109/TED.2013.2279021.
[30] Z. (Ashley) Jian, I. Sayed, W. Liu, S. Mohanty, E. Ahmadi, Characterization of MOCVD-grown AlSiO gate dielectric on β-Ga_2O_3 (001), Appl. Phys. Lett. 118 (2021) 172102, https://doi.org/10.1063/5.0048990.
[31] Y. Zhang, et al., Impact of surface treatments and post-deposition annealing upon interfacial property of ALD-Al_2O_3 on a-plane GaN, IEEE J. Electron Devices Soc. 8 (2020) 970–975, https://doi.org/10.1109/JEDS.2020.3020893.